Equivalent Gradient Area Based Fault Interpretation for Transformer Winding Using Binary Morphology

Huan Lin[1], Ziwei Zhang[2], Wenhu Tang[1], Qinghua Wu[1,2] and Jiudun Yan[2]

[1] School of Electric Power Engineering, South China University of Technology
Guangzhou, 510641, China
[2] Department of Electrical Engineering and Electronics
University of Liverpool, Liverpool L69 3GJ, U.K.

ABSTRACT

This paper proposes a novel fault interpretation method for transformer winding using features extracted from equivalent gradient areas of frequency responses. Firstly, frequency responses are pre-processed using binary morphology, aiming to eliminate the influence of stochastic factors such as noises and measurement configurations. Then pre-processed curves are divided into several frequency sub-bands, each of which reflects the influence of faults. Then fault features based on equivalent gradient areas are derived to quantify shape variations of frequency response curves with respect to specific fault types. Finally, real case studies are used to verify the capability of the proposed method, which can perform automated winding fault diagnosis.

Index Terms – **Transformer windings, fault diagnosis, frequency response, mathematical morphology.**

1 INTRODUCTION

ONCE transformers suffer from a failure, a power grid may break down leading to power interruption and huge economic losses [1]. Therefore, various diagnosis techniques have been developed to detect transformer faults and conduct maintenance work accordingly, in order to avoid severe mechanical or electrical failures. Among them the frequency response analysis (FRA) method draws broad attentions because of its effectiveness to detect structure changes of transformer windings. Usually, a FRA method assesses conditions of transformer windings by comparing measured frequency response (FR) curves with corresponding reference FRA curves. Since FRA curve shapes are determined by equivalent electrical parameters of windings, variations of FRA curves are able to reflect structure changes of windings.

In practice, both structure changes of windings and stochastic factors may change shapes of FRA curves. For example, the electromagnetic environment in substations is complex, and FRA measurements may be interfered by noises. Additionally measurement devices and measurement procedures of FRA are different, which also cause variations in FRA curves. Therefore, it is important to eliminate the influence of disturbances on FRA curves and preserve the frequency ranges with significant difference, which can improve fault diagnosis accuracies.

In addition, defining suitable frequency ranges for fault analysis can increase the sensitivity of winding fault indicators. In references [2, 3] it was stated that different equivalent electrical parameters influence different regions of FRA curves. By analyzing changes in different frequency regions, a winding deformation fault can be identified more accurately. For this reason, Ryder divided measurement frequency ranges into three sub-bands [4], and Sofian developed a division method using four sub-bands to quantify FRA effects of transformer winding and core [5]. However, the division ranges of the above sub-bands are fixed, which means that the ranges of these sub-bands cannot be adjusted dynamically according to FRA characteristics of transformers. As the sub-band ranges of various transformers are different, dynamic frequency region division methods were developed to divide frequency ranges. Velasquez developed an algorithm to divide the measurement frequency range into five sub-bands via analyzing real cases of transformer FRA curves [6], however this algorithm was too complicated. Gonzales proposed a dynamic division algorithm based on Velasquez's method, which is relatively simple. However, Gonzales's method separated different frequency regions based on the poles and zeros of FRA curves, which were difficult to be obtained in practice [7].

To quantify relative changes between FRA curves, statistic indicators are normally utilized [8]. However, statistic indicators can only represent the overall difference between FRA curves, while they are unable to describe how the curves move comparatively. Hence waveform indicators were developed, which are more appropriate to represent deviations between FRA curves [9]. Commonly, the sum of pole shifts and the sum of zero shifts between FRA curves

Manuscript received on 21August 2016, in final form 7 February 2017, accepted 3 March 2017. Corresponding author: W.H. Tang.

are chosen as the waveform indicators to describe changes between FRA curves, which have a clear physical meaning. The problem lies in that new resonant points may appear or disappear in measurement FRA curves compared with reference FRA curves. Moreover, not all the extreme points in FRA curves are poles or zeros, and some of them are just disturbances. Consequently, the pole and zero shifts are difficult to be calculated. Some researchers proposed to identify poles and zeros based on locations of phase crossing zero points. Nevertheless, there is no one to one correspondence between resonant points and phase zero crossing points. It indicates that it is impractical to employ shifts of poles and zeros as winding fault features. Thus a new type of fault indicators needs to be derived to represent deviations of FRA curves accurately.

In current FRA interpretations, FRA curves are analyzed by experienced electrical engineers and the deformation condition of a winding can be identified based on the difference between two FRA curves. However, this empirical approach has the following two drawbacks. Firstly, an analyst is required to have abundant experience of FRA interpretation and faults cannot be diagnosed by an inexperienced engineer. Secondly, different engineers could give different interpretations, as the relative movements between two FRA curves cannot be quantified effectively in the current practice. The main aim of the proposed approach is to automatically quantify the relationship between movements of FRA curves and winding faults, which can support fault diagnosis for inexperienced engineers in a unified framework.

The rest of this paper is organized as follows: Section 2 introduces the basic theory of binary morphology. Then an algorithm to pre-process FRA curves based on binary morphology is proposed in Section 3, which is employed to eliminate the effects of stochastic factors. Subsequently a dynamic sub-band division method based on the location of poles and zeros, as well as the magnitude deviation of FRA curves, is developed. In Section 4 a new kind of waveform indicators (i.e. equivalent gradient area parameters, EGAPs) is proposed, which can quantify the deviation of FRA curves accurately. Finally real case studies are investigated to demonstrate the ability of EGAPs to quantify variation features of FRA curves and achieve automated fault diagnosis. Concluding remarks are given in Section 7.

2 BINARY MORPHOLOGY

Mathematical morphology has been widely used in image processing, which utilizes the concepts in the set theory, geometry and topology to analyze the geometrical structure of images, in order to preserve the most important structure features in an image while eliminating stochastic factors (such as noises and rags) [10].

Initially, mathematical morphology was applied for processing of binary images, in which pixels have only two possible values “0” and “1”. Traditionally, the pixels with value “1” compose the object of interest, while the rest pixels constitute the background. Binary morphology considers a binary image as sets of elements, which have values “0” or “1”, then utilizes a structure element (SE) as a probe to detect the image structure. Given space limitations, only two primitive operations of binary morphology are introduced, i.e. dilation and erosion.

The dilation and erosion of an image A by a structure element B, which are denoted by $A \oplus B$ and $A \ominus B$ respectively, are defined as below.

$$A \oplus B = \left\{ c \in E^{N} \mid c = a + b, a \in A, b \in B \right\} \quad (1)$$

$$A \ominus B = \left\{ x \in E^{N} \mid x + b \in A, \forall b \in B \right\} \quad (2)$$

Dilation is mainly used for bridging gaps in an original image, while erosion is applied to eliminate irrelevant details in the original image and preserve important objects.

3 EXTRACTION OF AMPLITUDE DIFFERENCE BASED ON BINARY MORPHOLOGY

The causes of FRA curve variations are usually classified into three groups. The first kind of causes are stochastic factors such as noises, remanence conditions and measurement conditions, which lead to slight fluctuations. Different remanence conditions cause vertical displacement in low frequency ranges and horizontal shifts near the core anti-resonance peak, while curve differences are usually small [11]. The second one is the diversity of windings. FRA curves measured at windings of different phases or windings of the same type may manifest deviations due to the difference of flux paths and the different geometrical structure of transformers. The last one is the fault occurred in windings, leading to characteristic changes of FRA curve.

A severe deformation fault causes significant deviations in FRA curves, and other factors usually lead to comparatively slight deviations. Therefore, the frequency ranges with remarkable difference are the key features for fault diagnosis. For this reason, it is important to focus on those frequency ranges valuable for fault diagnosis and eliminate the influence of irrelevant factors. The disturbances in FRA curves are mainly in two forms. The first ones exist in the whole frequency range but have a relative low magnitude, and the other ones occur in some frequency points but have fast and small variations. In [12], discrete wavelet transform was applied to smooth FRA curves and preserve the information corresponding to power transformer internal faults, while all other disturbances were discarded. However, discrete wavelet transform is not able to eliminate noises, which cover the whole frequency range and have a relative low magnitude.

As mentioned in Section 2, the erosion of an image removes all structures that a SE fails to fit inside, and shrinks other regions while the essential shape characteristics of interest can be preserved. It is clear that the erosion operation meets the requirement of noise reduction for FRA curves if an appropriate SE is selected. Therefore erosion is applied to eliminate irrelevant details of FRA curves in this research.

Based upon the graphics theory, image blocks enclosed

by two FRA curves can be used for representing the difference between the two FRA curves. The bigger are the areas of the enclosed image blocks, the more significant is the variation between FRA curves. Furthermore, the amplitude difference represented by blocks can be processed based on an image processing technique. By filtering out blocks with smaller areas, the interference of irrelevant factors is reduced to some extent. At the same time the blocks representing significant amplitude deviations are preserved for further analysis.

In [13], the authors stated that the erosion operation combined with small area filtering was able to eliminate irrelevant details. This method is used for FR data pre-processing in the following subsections. Firstly a set of FRA curves is transformed into a binary image. Then the erosion operation is applied to process the image. Subsequently the blocks, whose areas are smaller than a pre-set threshold, are removed and significant amplitude differences are extracted in the form of image blocks. To determine the values of the SE and the area threshold, 22 sets of FR measurements of different transformers with multiple faults are utilized, which are collected from two grid companies and other literatures.

3.1 BINARYZATION OF RESPONSE CURVES

In this research, FRA curves are transformed into binary images before being processed by binary morphology. Consider a FRA curve has I data points $p_i\ (f_i, m_i)$, where f_i is the frequency value of ith data point and m_i is the corresponding magnitude. Firstly a matrix which has a suitable size $W \times H$ is built according to the amplitude and frequency ranges of FR data, where W and H correspond to the width and height of the produced image. In this research, W is set to 1200 pixels and H is set to 900 pixels. As the frequency range of the obtained FR data is between 20 Hz and 2 MHz, the chosen W and H are sufficient to preserve the value and shape information provided by the FR data in the binary images while the computation complexity is acceptable.

Then for every data point p_i in the FRA curve, its corresponding coordinates in the matrix are calculated by Equations (3) and (4), where [] is the rounding operator. Therefore coordinates (x_{ri}, y_{ri}) and (x_{mi}, y_{mi}) can be obtained, which represent the locations of the reference FRA curve and the measurement FRA curve respectively in every column of the matrix. For every column, the values of matrix elements, whose vertical coordinate values are between y_{ri} and y_{mi}, are specified as "1" and the others are set to "0". After that a binary image representing the amplitude difference of FRA curves is formed.

$$x_i = \left[\frac{\log_{10}(f_i) - \log_{10}(f_1)}{\log_{10}(f_I) - \log_{10}(f_1)} \times W \right] \quad (3)$$

$$y_i = \left[\frac{m_i - m_1}{m_I - m_1} \times H \right] \quad (4)$$

For example, measurements on a HV winding of a transformer which suffers from radial deformation is in Figure 1, while its reconstructed binary image is in Figure 2.

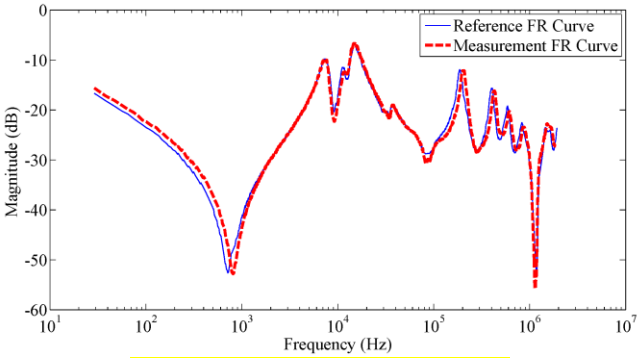

Figure 1. An example of FR measurements.

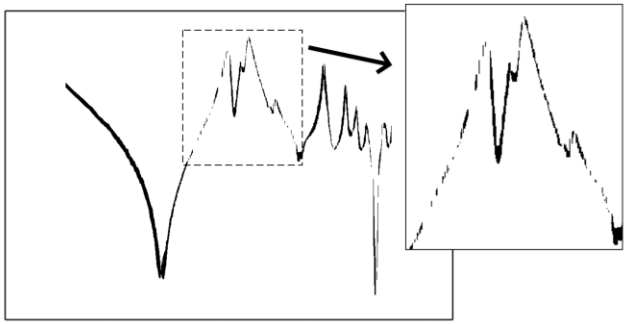

Figure 2. The binaryzation image corresponding to Figure 1.

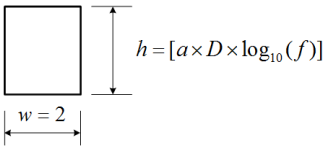

Figure 3. The proposed structure element.

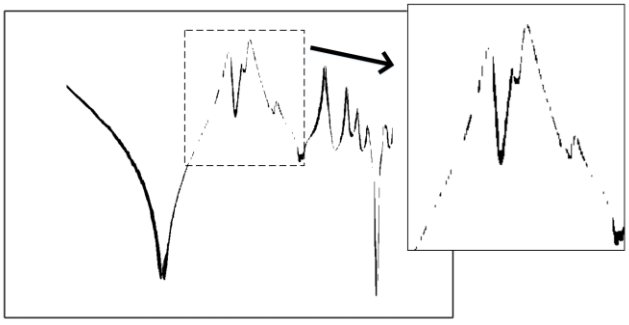

Figure 4. Eroded image of Figure 2 using the proposed structure element.

3.2 DERIVATION OF A STRUCTURE ELEMENT FOR EROSION OPERATION

When applying image erosion, a SE is the key factor influencing the result of image processing. The selection of SE mainly focuses on selecting the shape and the size of SE.

How to select the shape of the SE usually depends on the geometric shapes, which are to be eliminated from an original image. While the primary goal of morphological operations is to remove small angular features and thin lines from the image, a square or rectangular element is recommended. In FRA curves, noisy details mainly contain random fluctuations and fixed errors, which manifest as

glitches and thin lines. Therefore a rectangle SE is chosen for erosion operations in this research.

Generally, the height of the SE usually takes 1% to 5% of the height of the processed curve. The disturbances in FRA curves related to the change of measurement conditions mainly occur in the high frequency region, while fault features are more abundant in the low and medium frequency regions. Consequently a SE, whose size varies according to amplitude ranges and frequency response data being processed, is proposed in Figure 3.

The definition of this rectangle SE is $w \times h$, where w and h are the width and height of the SE respectively. The height h is set as $h = [a \times D \times \log_{10}(f)]$. Here a is a coefficient needed to be specified on previous experience and multiple trials. D is the subtraction of the global maximum and minimum between the reference and measurement curves, i.e. the height of FRA curves. f is the frequency value of frequency response data processing, while $[]$ is the round operator.

Determining the specific size of a SE is mostly an empirical process. The selection of the size relates to the desired processing effect. When the size of a SE is bigger, the processed image shrinks more. To determine the specific parameters of the SE in this proposed approach, the value of the parameter a is altered from 1% to 5% by a step of 1%, and the value of w is altered from 1 to 3 by a step of 1. Then the generated SEs are applied to erosion operations for 22 cases of FR measurements. After comparison of these SEs, a is set to 0.01 and w is set to 2, as the corresponding SE provides the best erosion results. The erosion results of Figure 2 using the proposed SE is illustrated in Figure 4.

3.3 PRE-SET AREA THRESHOLD

As shown in Figure 4, large image blocks are preserved after the erosion operation. These image blocks represent the remarkable differences between two FR measurements, which can reveal the type of fault and its severity. Meanwhile small blocks are eroded into a few smaller isolated blocks. To avoid the interference of these irrelevant details for fault diagnosis, an area threshold is set and the blocks whose areas are smaller than the threshold are filtered out.

As the size of the proposed SE varies according to the height of curves, the area threshold should also be adjusted corresponding to different erosion results. Consequently, the area threshold S_t is set as $S_t = b \times D$ and D is the height of FRA curves. In this research, 22 sets of FR measurements of different transformers with faults are employed, which are collected from two grid companies and other literatures. These measurements are utilized to determine the value of the parameter b. The value of b is altered between 0.1 and 1 by a step of 0.1. Different filtering results of the calculated area thresholds in 22 cases are compared. When b is set to 0.3, the filtering result is the best, i.e. the fault features are preserved and irrelevant details are eliminated in most cases.

After the filtration of the isolated small image blocks, the remaining regions after the erosion and filtration are restored to the original size by dilation, to avoid excessive processing of fault features.

The final processing result using the binary morphology is shown in Figure 5. It is noticed that the frequency ranges reflecting remarkable amplitude difference can be acquired by the developed pre-processing method, which provides a solid foundation for the following analysis.

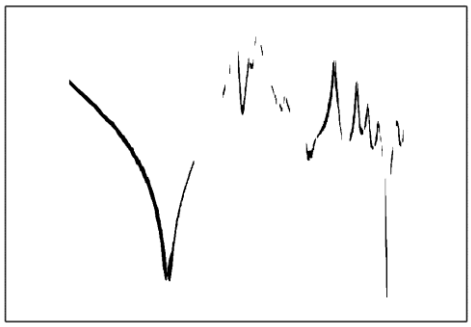

Figure 5. The final processing result of Figure 1.

4 DYNAMIC REGION DEFINITION OF FR BASED ON LOCATIONS OF RESONANCE AND AMPLITUDE DIFFERENCE

As stated previously, analyzing FRA curves in divided frequency regions can increase the sensitivity of indicators to winding faults. As a result, a reliable frequency region division method can effectively improve the accuracy of fault diagnosis. Motivated by this, a novel frequency region division method is proposed and illustrated in Figure 6.

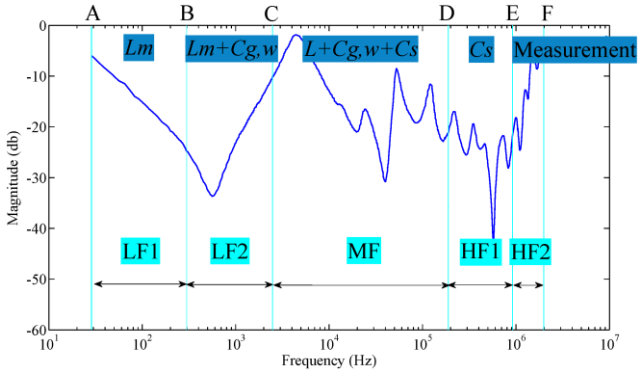

Figure 6. The frequency division sub-bands using the proposed method.

Recent studies reported that a FRA curve can be divided into five regions [6, 7]. As shown in Fig 6, the sub-band LF1 is between A and B, dominated by the magnetization inductance L_m. The region between B and C (i.e. LF2) is mainly influenced by the shunt capacitance $C_{g,w}$. The frequency region between C and D is defined as the sub-band MF, which describes interactions among windings. Hence this area is sensitive to the winding bulk movement. The sub-band HF1 between D and E reflects the strong capacitance response caused by the series capacitance C_s, therefore the FR in this part is very sensitive to localized

changes of windings. Finally, in the sub-band HF2, the FR manifests characteristics of inductive impedance, which is influenced by the inductance of internal leads of transformers and grounding leads.

As shapes of FRA curves are related to physical components of a transformer (e.g. winding, core, lead and tap), frequency division points of various regions for different curves are unique. Therefore, dividing FRA curves according to their individual characteristics is more feasible. However, there are no widely accepted division method.

In [6, 7], a method was attempted to divide FRA curves based on locations of poles and zeros. However, as discussed above, detecting all the locations of resonant points is infeasible. To overcome such drawbacks of current methods, this research only utilizes the location of the first pole and the first zero along with FRA curve amplitude differences, which aims to avoid the difficulty in identifying all poles and zeros in medium and high frequency regions.

According to [3], the first zero of a FRA curve is usually formed because of the interaction of L_{m} and $C_{\mathrm{g,w}}$, while the first pole is formed due to the shunt resonance of L and $C_{\mathrm{g,w}}$. Both of these resonant points can be recognized easily from FRA curves, therefore they are defined as the reference points for separating LF1, LF2 and MF. When determining the first zero, the double peak phenomenon, which is due to different magnetic paths between a lateral winding and a central winding, is considered [14]. The real zero point can be identified by comparing the amplitudes of these two minimums. The detailed procedure of determining the division points A, B, C of the low and medium frequency ranges is depicted in Figure 7, where $f = m(s)$ is the frequency value of the sth measured FR data point.

In Figure 6, variations of FRA curves in different frequency regions are dominated by different equivalent electrical parameters, and FRA curve variations in a frequency region are mainly caused by the change of dominating parameters, while the influence of other parameters is generally small. Therefore the medium and high frequency regions can be divided according to the distribution of amplitude differences.

- Firstly the graphics based method, proposed in section 3.1, is utilized to acquire a binary image, which preserves frequency ranges with comparatively significant amplitude differences. Then two searching ranges are defined according to characteristics of multiple FRA curves. In the searching ranges, the binary image is searched column by column from the right to the left, to find out whether any image block exists for every frequency point (i.e. a column in the binary image matrix corresponding to the currently searching frequency). When consecutive multiple frequency points have image blocks, according to the above analysis, these frequency points belong to the same sub-band. If a frequency point i without any image blocks is firstly identified in a searching range, it means that at this frequency point i and at least one left adjacent frequency point (as the width of the SE is 2), the reference FRA curve and the measurement FRA curve have the same magnitude after eliminating the influence of noises and some stochastic factors by morphological operations. In other words, in these frequency points the FRA curves are not influenced by the changed electrical parameter any more, which is probably because they are in another sub-band which is not dominated by this electrical parameter. Therefore, the corresponding frequency value of point i is defined as the separation frequency between two sub-bands.
- However, if the equivalent electrical parameters dominating a sub-band are changed significantly, the sub-bands nearby may also be influenced. As a result, image blocks may always exist in the whole searching range. In other words, the separation point between sub-bands cannot be determined by searching the frequency point without significant amplitude differences. In this case which has relatively low presence probability, fixed frequency points for dividing the medium and high frequency regions are employed. These fixed division points are defined after modifying the methods in [3] and [14] and analyzing multiple FRA curves, which have pre-defined reference values. The detailed process of finding the division points D, E, F are explained in Figure 8, where $f = m(s)$ is the corresponding frequency value of the sth frequency point in a FRA curve.

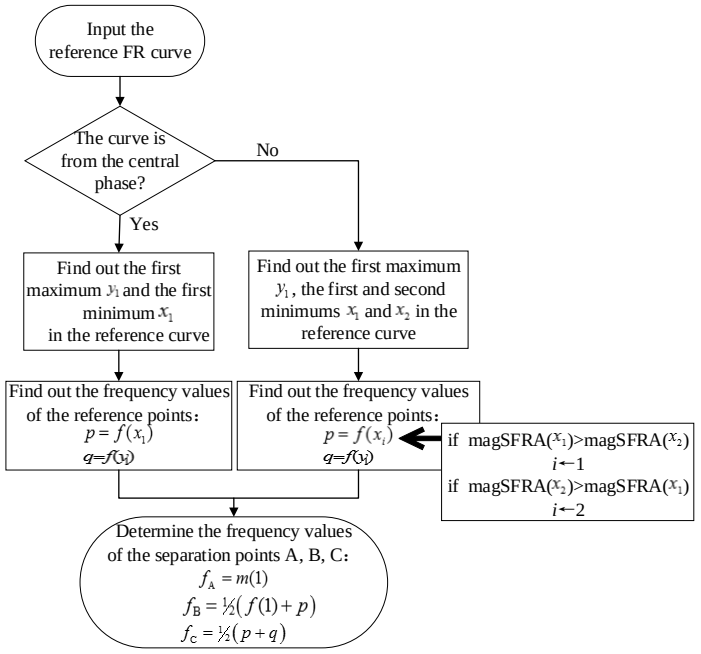

Figure 7. The procedure of defining the division points A, B and C.

The proposed method has been compared with Velasquez's method and Gonzales's method. Figure 9 shows the FR measurements of a transformer winding suffering from mechanical deformation, and the division results of all the three methods are also presented.

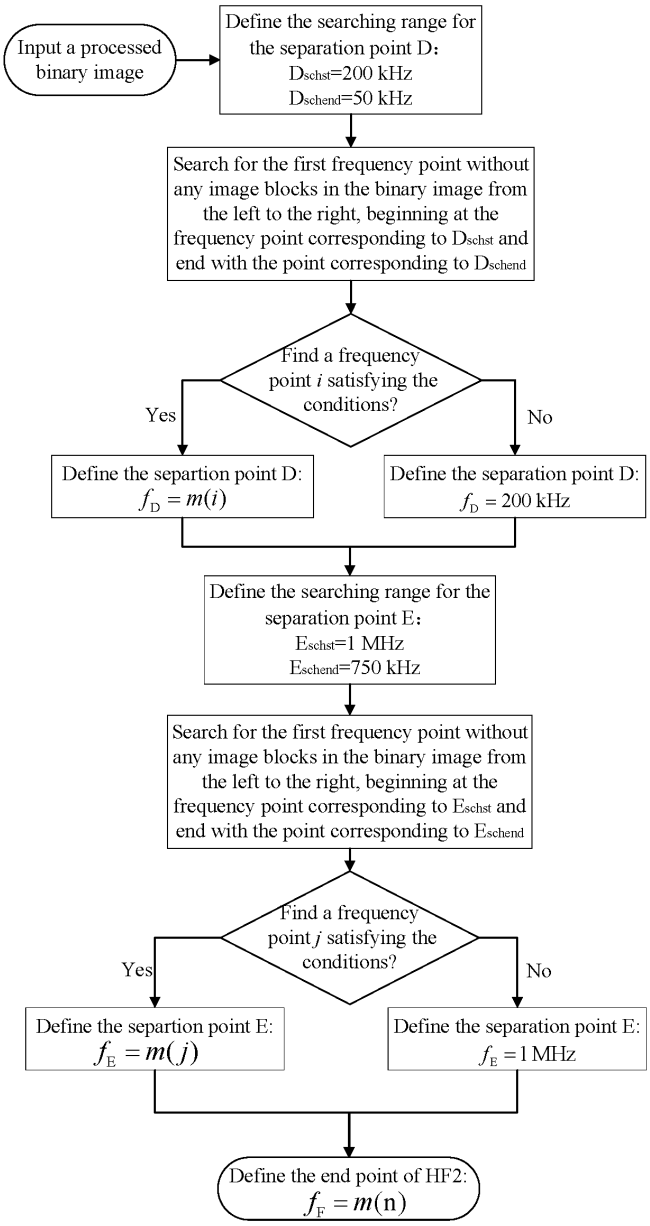

Figure 8. The procedure of defining division points D, E and F.

- The division points of LF1 and LF2 defined by these three methods are nearly the same. The separation points of LF2 and MF chosen by the methods have large differences. The proposed method defines the separation point C based on the location of the first pole, which is utilized to distinguish the influence of L_m and L. Velasquez summarized the resonance peak distributions from four sets of FR measurements, and determines the location of point C based on the frequency value of the first pole. Gonzales separated LF2 and MF according to the location of the second pole, but without a sufficient explanation.
- The division point D determined by the proposed method is close to Velasquez's, while Gonzale's is different. It is seen that FRA curves have significant variations in the range from 200 to 400 kHz. According to the proposed method and Velasquez's method, these variations are categorized into HF1. However, Gonzales classified them into MF, which may lead to misclassification. The proposed method is similar to Velasquez's method for separating HF1 and HF2, which is different from Gonzales's method.

In summary, the proposed dynamic frequency region division method is a compromise of accuracy and feasibility. In the following sections, FRA curves are analyzed in sub-bands defined by the proposed dynamic division method.

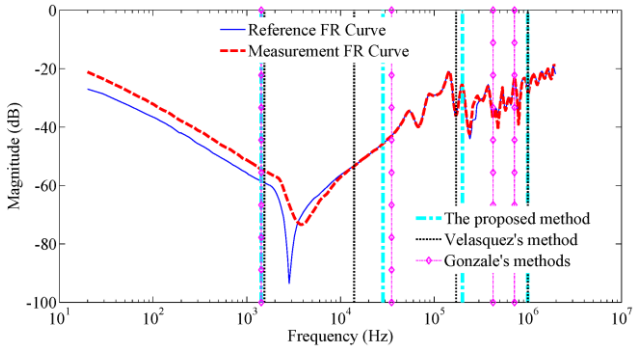

Figure 9. Result comparison among three dynamic division methods.

5 EQUIVALENT GRADIENT AREA PARAMETER FOR DETERMINING CURVE DEVIATION OF FR

To overcome the aforementioned drawbacks of the existing statistic indicators and waveform features, a new kind of parameters is proposed to quantify deviations between curves more accurately. In biology, differences between gene curves are detected by computing the areas between curves [16], while in this research the determination of curve shift direction is very important. Inspired by this quantification method, the areas between curves and the slopes of curves are taken into account for quantifying curve variations. Then a series of equivalent gradient area parameters (EGAPs) are derived to quantify curve deviations between two FRA curves including the movement direction and the extent of variations.

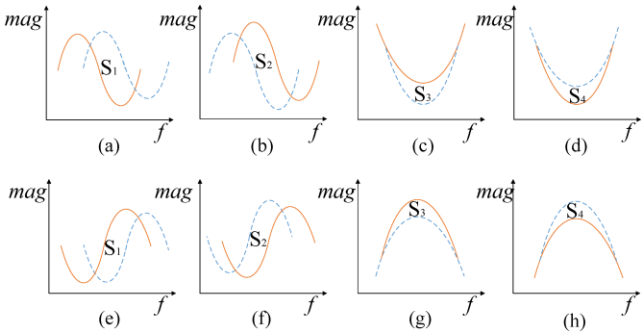

Figure 10. 8 typical cases of sinusoid movements.

In the semi-log coordinate, a FRA curve around a pole or a zero can be approximated as parts of a sinusoid, and the definition of EGAPs are derived by analyzing the relationships of the areas enclosed by two sinusoids, the mean slopes of curve segments between two intersections and the segment comparative movements, while the relative

position of two sinusoids is different. Figure 10 illustrated eight typical positions of a sinusoid displaced to another sinusoid. The sinusoids in orange represent reference FRA curves C_{ref} , and blue ones are measurement FRA curves C_{crt} .

Firstly, the enclosed area S of two curve segments between two intersections of the reference FRA curve and the measurement FRA curve is defined in equation (5). Then G_{mref} and G_{mcrt} , which are the mean slopes of the curve segments between intersections, are specified in equations (6) and (7), where $mag_{\text{ref}}(i)$ and $mag_{\text{crt}}(i)$ are the amplitude values of the ith data point in the reference FRA curve segment and the measurement FRA curve segment between the intersections respectively. $f(i)$ is the frequency value of the ith data point, and the data points between the intersections sampled by the FRA instrument are n.

$$S = \sum_{i=1}^{\text{n-1}} \frac{1}{2}(f(i+1)-f(i))*\big((mag_{\text{crt}}(i)-mag_{\text{ref}}(i)) + (mag_{\text{crt}}(i+1)-mag_{\text{ref}}(i+1))\big) \quad (5)$$

$$G_{\text{mref}} = \frac{1}{\text{n-1}} \sum_{i=1}^{\text{n-1}} \frac{mag_{\text{ref}}(i+1)-mag_{\text{ref}}(i)}{\log_{10} f(i+1)-\log_{10} f(i)} \quad (6)$$

$$G_{\text{mcrt}} = \frac{1}{\text{n-1}} \sum_{i=1}^{\text{n-1}} \frac{mag_{\text{crt}}(i+1)-mag_{\text{crt}}(i)}{\log_{10} f(i+1)-\log_{10} f(i)} \quad (7)$$

Table 1. Relationships of S , G_{mref} , G_{mcrt} and the curve segment movement direction.

Instance	S	G_{mref}	G_{mcrt}	Movement Direction
8 (a)	$S > 0$	$G_{\text{mref}} < 0$	$G_{\text{mcrt}} < 0$	Shift rightwards
8 (b)	$S < 0$	$G_{\text{mref}} < 0$	$G_{\text{mcrt}} < 0$	Shift leftwards
8 (c)	$S < 0$	$G_{\text{mref}} \approx 0$	$G_{\text{mcrt}} \approx 0$	Move upwards
8 (d)	$S > 0$	$G_{\text{mref}} \approx 0$	$G_{\text{mcrt}} \approx 0$	Move downwards
8 (e)	$S < 0$	$G_{\text{mref}} > 0$	$G_{\text{mcrt}} > 0$	Shift rightwards
8 (f)	$S > 0$	$G_{\text{mref}} > 0$	$G_{\text{mcrt}} > 0$	Shift leftwards
8 (g)	$S < 0$	$G_{\text{mref}} \approx 0$	$G_{\text{mcrt}} \approx 0$	Move upwards
8 (h)	$S > 0$	$G_{\text{mref}} \approx 0$	$G_{\text{mcrt}} \approx 0$	Move downwards

In Table 1, the relationships of area S , the mean slopes G_{mref} , G_{mcrt} and the curve segment movement direction are listed. It can be found that there are some links between S , G_{mref} , G_{mcrt} and the curve segment movement direction, which can be summarized as following, where G_{m} is G_{mref} or G_{mcrt} depending on which has a greater absolute value.

- While G_{m} is much greater than zero, $S_{\text{c}} = S * G_{\text{m}}$ is defined. If $S_{\text{c}} < 0$, the curve segment shifts to the right, otherwise the curve segment shifts to the left.
- While G_{m} is close to zero, if $S < 0$, the curve segment moves upwards, otherwise the curve segment moves downwards.

As a result, four types of area parameters are defined in equation 8, to describe the displacement of curve segments between two intersections. S_1 represents the extent of a curve moving rightwards, while S_2 represents the extent of moving leftwards. S_3 and S_4 describe the curve segment moving upwards or downwards respectively.

$$\begin{aligned} &S_1 = |S|, S_2 = 0, S_3 = 0, S_4 = 0, \quad if \quad S_c < 0 \\ &S_2 = |S|, S_1 = 0, S_3 = 0, S_4 = 0, \quad if \quad S_c > 0 \\ &S_3 = |S|, S_1 = 0, S_2 = 0, S_4 = 0, \quad if \quad G_m \approx 0 \quad \& \quad S > 0 \\ &S_4 = |S|, S_1 = 0, S_2 = 0, S_3 = 0, \quad if \quad G_m \approx 0 \quad \& \quad S < 0 \end{aligned} \quad (8)$$

In real cases, the variation trends of FRA curves are more complicated than that of sinusoids. In addition to curve shifts, the asymmetry of curve segments may also lead to the non-zero value of G_{m} . To prevent the asymmetry of a curve segment from influencing the judgement on how the curve segment comparatively moves, a slope threshold T is defined to specify when the curve segment is considered to move upwards or downwards. If the absolute values of G_{mref} and G_{mcrt} are both less than the threshold, the curve segment is considered only to move upwards or downwards, otherwise it is considered to move leftwards or rightwards.

The procedure of determining the value of T is described as below: The slope threshold T is assigned to different integer values from 7 to 15 by a step of 1. When T takes a certain value, all ERGPs for different frequency regions of the 22 cases are calculated. The curve movements are evaluated according to ERGPs, and the analysis results are compared with visual observations. When T is set to 10, all the evaluated results are consistent to the visual observation. Therefore the slope threshold T is set to 10 in the proposed approach.

Table 2. The EGAPs for Figure 1.

Sub-band	S_{r1}	S_{r2}	S_{r3}	S_{r4}
LF1	0.0303	0	0	0
LF2	0.0157	0	0	0
MF	0.00261	0.0006	0.0027	0.00006
HF1	0.0361	0	0	0
HF2	0	0.0179	0	0.01

As the frequency ranges of different sub-bands have different sizes, the area parameters S_1 , S_2 , S_3 and S_4 of different sub-bands cannot be quantified under a normalized numerical range. Therefore the averaged EGAPs S_{ri} are defined to describe relative deviations of FRA curves in various sub-bands, where f_{substart} and f_{subend} are the frequency values of the start point and the end point of a sub-band. max_{global} and min_{global} are the global maximum and minimum of the reference FRA curve and the measurement FRA curve. Assuming that the number of curve segments in a sub-band is m.

Using Equation 9, the EGAPs which represent the deviations of FRA curves can be calculated, then the specific type of winding faults can be identified according to the distribution characteristics of various EGAPs in

relevant sub-bands.

$$S_{ri} = \sum_{i=1}^{m} S_i \Big/ (f_{\text{subend}} - f_{\text{substart}}) * (\max_{\text{global}} - \min_{\text{global}}) \quad (9)$$

The corresponding EGAPs of Figure 1 are shown in Table 2. According to the calculated EGAPs, the measurement FRA curve shifts to the right compared with the reference FRA curve in LF1 and LF2. In MF, the deviation of curves is slight. In HF1, the measurement FRA curve shifts to the right. And in HF2, the EGAPs illustrate that there are some curve segments shifting to the left or moving upwards. All these curve segment movement trends are consistent with the actual variations of the FRA curves, which demonstrates the detection ability of EGAPs to describe FRA curve movements.

6 VALIDATION AND DISCUSSION

The proposed winding fault interpretation algorithm is validated by two real typical cases from a FR database.

Case 1: This case corresponds to a HV winding of a 110/10 kV transformer. The reference test on this winding was measured when the transformer was healthy, while the actual test was performed on the transformer suffering an axial displacement. The FR traces are shown in Figure 11.

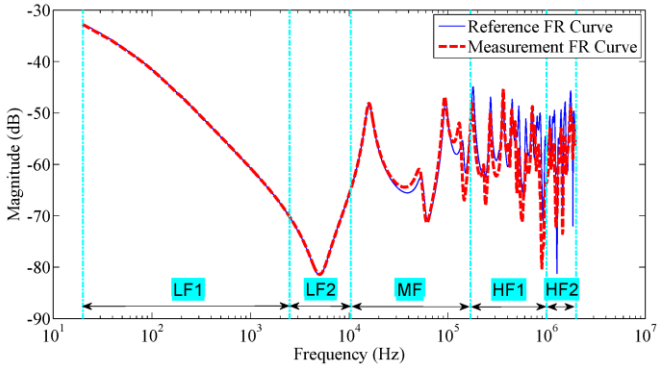

Figure 11. FR measurements on an HV winding of a 110/10 kV transformer.

Applying the pre-processing procedure based on the binary morphology and the dynamic frequency region division method, the calculation results of the EGAPs for this case are listed in Table 3. It can be seen that S_{r1}, S_{r2}, S_{r3} and S_{r4} are all close to zero in the sub-bands LF1 and LF2, which means that the measurement FRA curve and the reference FRA curve are nearly the same in these two sub-bands. In MF, S_{r2} and S_{r4} are predominated, which can be inferred that the measurement FRA curve shifts leftwards as well as moves upwards slightly compared with the reference FRA curve. In HF1, S_{r2} and S_{r3} are much greater than S_{r1} and S_{r4}. It illustrates that the measurement curve comparatively shifts leftwards and moves downwards. In HF2, the measurement curve slightly moves leftwards, rightwards, as S_{r1}, S_{r2} has much greater value than others. It is noticed that the identification of the EGAPs is in line with the actual variations between the two FRA curves.

Table 3. The EGAPs for Figure 11.

Sub-band	S_{r1}	S_{r2}	S_{r3}	S_{r4}
LF1	0	0.0001	0	0
LF2	0	0	0	0
MF	0	0.0139	0	0.0102
HF1	0.004	0.0423	0.0399	0
HF2	0.0088	0.0187	0.0018	0

Table 4. Comparison of the EGAPs and descriptions from other literatures for axial displacement.

Sub-band	EGAPs	Other literature [3] [5]
LF1	Ignorable deviations	Generally unaffected
LF2	Ignorable deviations	Generally unaffected
MF	Shift leftwards and move downwards slightly	Obvious changes (usually shift leftwards)
HF1	Shift leftwards and move upwards	Obvious changes (usually shift leftwards)
HF2	Slightly moving leftwards, rightwards	Unpredictable

Moreover, the identification of EGAPs in this case is also compared with the qualitative rules of winding axial displacement from other researchers' work, as well as some international technical standards as listed in Table 4. It can be noted the identification of the EGAPs and other literatures are basically consistent, except the differences in the sub-band HF2, which may be caused by the influence of experiment configurations.

Case 2: This case corresponds to a 138/13.8 kV power transformer. FR measurements were recorded in the high voltage winding of phase A, which is shown in Figure 12. According to the onsite diagnosis, the deviations between curves are mainly due to short-circuit between turns, and the fluctuations in HF2 probably relates to stochastic factors. The calculated results of EGAPs are listed in Table 5, which is basically consistent to the deviations between FRA curves. Moreover, the identification of EGAPs for shorted turns are compared with diagnosis rules from other literatures as listed in Table 6, which are nearly the same.

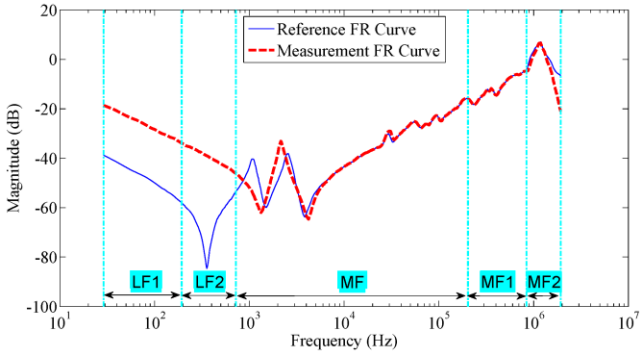

Figure 12. FRA in an HV winding of a 138/13.8 kV transformer.

It can be summarized from the above cases that EGAPs have the ability to perform automated winding fault diagnosis. To identify a specific winding fault, EGAPs of FRA curves are calculated and compared with diagnosis results based on distributions of EGAPs. The most

important contribution of this research is on the derivation of EGAPs to quantify FRA curve trends accurately, so as to achieve automated fault diagnosis, which overcomes the difficulties of parameter calculations in traditional algorithms. Additionally, EGAPs can quantitatively identify faults, unlike the ambiguous descriptions from traditional diagnosis rules. Therefore, EGAPs can be utilized as a new kind of quantitative tool to accurately identify winding deformation faults, which is very useful for analyzing characteristics of faults more accurately.

Table 5. The EGAPs for Figure 12.

Sub-band	S_{r1}	S_{r2}	S_{r3}	S_{r4}
LF1	0.2523	0	0	0
LF2	0.2505	0	0	0
MF	0	0.0016	0.0003	0.0001
HF1	0	0.0002	0	0
HF2	0.0045	0	0.0362	0

Table 6. Comparison of EGAPs and diagnosis rules from other literatures for shorted turns.

Sub-band	EGAPs	Other literature [15] [17]
LF1	Shift rightwards greatly	Increased amplitude and shift rightwards
LF2	Shift rightwards greatly	Increased amplitude and shift rightwards
MF	Ignorable deviations	Generally unaffected
HF1	Ignorable deviations	Generally unaffected
HF2	Move downwards	Generally unaffected

7 CONCLUSION

This paper proposes a novel interpretation algorithm of FR measurements for winding fault diagnosis. Binary morphology is utilized to eliminate irrelevant details in FR measurements and preserve significant amplitude differences representing key features of FRA curves. A new dynamic frequency region division method is also developed, which shows a high accuracy and feasibility compared with conventional division methods. To overcome the drawbacks of statistic indicators and waveform features, EGAPs are defined to represent the deviation of FRA curves more accurately, which can be applied for automated winding fault diagnosis. Moreover, EGAPs are able to represent diagnosis rules in a quantitative way, which contributes to analyzing characteristics of winding faults more accurately.

8 ACKNOWLEDGMENT

The project is supported by the National Natural Science Foundation of China (No. 51477054) and the National High Technology Research and Development Program of China (863 Program) (No. 2015AA050201).

REFERENCES

[1] J. A. S. B. Jayasinghe, Z. D. Wang; P. N. Jarman, A. W. Darwin, "Winding movement in power transformers: a comparison of FRA measurement connection methods," IEEE Trans. Dielectr. Electr. Insul., Vol. 13, No. 6, pp. 1342-1349, 2006.

[2] A. Shintemirov, W. H. Tang, and Q. H. Wu, "Transformer winding condition assessment using frequency response analysis and evidential reasoning," Electric Power Applications, IET, Vol. 4, pp. 198–212, 2010.

[3] N. Hashemnia, A. Abu-Siada and S. Islam, "Improved power transformer winding fault detection using FRA diagnostics - part 2: radial deformation simulation," IEEE Trans. Dielectr. Electr. Insul., Vol. 22, No. 1, pp. 564 - 570, 2015

[4] S. A. Ryder, "Diagnosing transformer faults using frequency response analysis," IEEE Electr. Insul. Mag., Vol. 19, No. 2, pp. 16–22, 2003.

[5] D. M. Sofian, *Transformer FRA Interpretation for Detection of Winding Movement*, Ph.D. dissertation, The University of Manchester, UK, 2007.

[6] J. Velasquez and D. Kolb, "Identification of transformer-specific frequency sub-bands as basis for a reliable and automatic assessment of FRA results," Conf. Condition Monitoring and Diagnosis, (CMD). Tokyo, Japan, pp. 1-6, 2010.

[7] J. Gonzales and E. Mombello, "Automatic detection of frequency ranges of power transformer transfer functions for evaluation by mathematical indicators," IEEE 6th Power Energy Soc. (PES) Transmission and Distribution: Latin America Conf. Exposition (T&D-LA), pp. 1–8, 2012.

[8] J. C. G. Arispe and E. E. Mombello, "Detection of failures within transformers by FRA using multiresolution decomposition," IEEE Trans. Power Delivery, Vol. 29, pp. 1127–1137, 2014.

[9] E. Rahimpour and D. Gorzin, "A new method for comparing the transfer function of transformers in order to detect the location and amount of winding faults," Electr. Eng., Vol. 88, No. 5, pp. 411–416, 2006.

[10] Q. H. Wu, Z. Lu, and T. Y. Ji, *Protective Relaying of Power Systems using Mathematical Morphology*". Springer, 2009.

[11] N. Abeywickrama, Y. Serdyuk, and S. Gubanski, "Effect of core magnetization on frequency response analysis (FRA) of power transformers," IEEE Trans. Power Delivery, Vol. 23, No. 3, pp. 1432–1438, 2008.

[12] J. C. Gonzales and E. E. Mombello, "Fault Interpretation Algorithm Using Frequency-Response Analysis of Power Transformers." IEEE Trans. Power Delivery, Vol. 31, No. 3, pp.1034–1042, 2016.

[13] Y. Xu, Y. Gong, Y. Liu, W. Ma, Q. Zhao, and W. Wang, "Transformer winding frequency response data analysis based on block frequency point method," Automation Electr. Power Syst., Vol. 38, No. 6, pp. 91–97, 2014.

[14] D. M. Sofian, Z. Wang, and J. Li, "Interpretation of transformer FRA responses: Part II: influence of transformer structure," IEEE Trans. Power Delivery, Vol. 25, No. 4, pp. 2582–2589, 2010.

[15] J. Velasquez, *Intelligent Monitoring and Diagnosis of Power Transformers in the Context of an Asset Management Model*," Ph.D. dissertation, Polytechnic University of Catalonia, 2013.

[16] C. Minas, S. Waddell, and G. Montana, "Distance-based differential analysis of gene curves," Bioinformatics, Vol. 27, No. 22, pp. 3135–141, 2011.

[17] P. Picher, J. Lapworth, T. Noonan, J. Christian, and Others, "Mechanical condition assessment of transformer windings using frequency response analysis," CIGRE Working Group A, vol. 2, 2006.

H. Lin was born in Swatow, China in 1989. He received the B.Eng. and M.Sc. degrees from South China University of Technology, Guangzhou, China, in 2012 and 2015, respectively. His research interests include power transformer condition assessment, machine learning and signal processing. He is currently an electrical engineer in Swatow Electric Power Supply Bureau of Guangdong Power Grid Co., Ltd., China.

Z.W. Zhang received the B.Eng. and Ph.D. degrees from the University of Liverpool, Liverpool, U.K., in 2011 and 2016, respectively. She is currently working as a post-doctoral research assistant at Department of Electrical Engineering, State Key Laboratory of Control and Simulation of Power System and Generation Equipment, Tsinghua University, Beijing, China. Her research interests include fault diagnosis and condition monitoring of high-voltage apparatus.

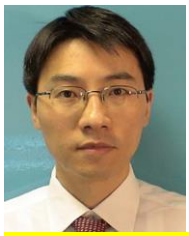

W.H. Tang (M'05-SM'13) received the B.Eng. and M.Sc. degrees in electrical engineering from Huazhong University of Science and Technology, Wuhan, China, in 1996 and 2000, respectively, and the Ph.D. degree in electrical engineering from The University of Liverpool, Liverpool, U.K., in 2004. He was a Postdoctoral Research Assistant and subsequently a Lecturer at The University of Liverpool between 2004 and 2013. In April 2013, he joined South China University of Technology, China, to take up his appointment as a Distinguished Professor in the School of Electric Power Engineering. He has authored and coauthored more than 80 technical publications, including 35 journal papers and 1 research monograph published by Springer. His research interests are wind power generation and control, condition monitoring and fault diagnosis of power apparatus, multiple criteria decision analysis and intelligent decision support systems.

Q.H. Wu (M'91–SM'97–F'11) received the Ph.D. degree in electrical engineering from The Queen's University of Belfast (QUB), Belfast, U.K., in 1987. He was a Research Fellow and subsequently a Senior Research Fellow in QUB from 1987 to 1991. He joined the Department of Mathematical Sciences, Loughborough University, U.K., in 1991, as a Lecturer; subsequently he was appointed a Senior Lecturer. In September, 1995, he joined The University of Liverpool, Liverpool, U.K., to take up his appointment to the Chair of electrical engineering in the Department of Electrical Engineering and Electronics. He is also with the School of Electric Power Engineering, South China University of Technology, Guangzhou, China, as a Distinguished Professor and the Director of Energy Research Institute of the University. He has authored and coauthored more than 440 technical publications, including 240 journal papers, 20 book chapters, and 3 research monographs published by Springer. He is a Fellow of IET, Chartered Engineer and Fellow of InstMC. His research interests include nonlinear adaptive control, mathematical morphology, evolutionary computation, power quality, and power system control and operation.

J.D. Yan received his B.Sc. and M.Sc. degrees from Tsinghua University (Beijing) in 1986 and 1988 respectively, and obtained his PhD degree at the University of Liverpool in 1998. Since then he has been working in the University of Liverpool and currently Reader in Electrical Engineering. His research interests include switching arcs, plasma physics, SF6 replacement, and more recently intelligent electrical apparatus for use in smart grid.